Research Article Vol. 30, No. 8 / 11 Apr 2022 / Optics Express 13121
Optics EXPRESS

Deep learning-based ballistocardiography reconstruction algorithm on the optical fiber sensor

SHUYANG CHEN,[1] FENGZE TAN,[2] WEIMIN LYU,[2] HUAIJIAN LUO,[1] JIANXUN YU,[3] JIAQI QU,[1] AND CHANGYUAN YU[1,*]

[1]*Photonics Research Center, Department of Electronic and Information Engineering, The Hong Kong Polytechnic University, Hong Kong, China*
[2]*Shenzhen Research Institute, The Hong Kong Polytechnic University, Shenzhen, China*
[3]*Photonics Research Center, Department of Electrical Engineering, The Hong Kong Polytechnic University, Hong Kong, China*
[*]*Changyuan.yu@polyu.edu.hk*

Abstract: Ballistocardiography (BCG) is a vibration signal related to cardiac activity, which can be obtained in a non-invasive way by optical fiber sensors. In this paper, we propose a modified generative adversarial network (GAN) to reconstruct BCG signals by solving signal fading problems in a Mach-Zehnder interferometer (MZI). Based on this algorithm, additional modulators and demodulators are not needed in the MZI, which reduces the cost and hardware complexity. The correlation between reconstructed BCG and reference BCG is 0.952 in test data. To further test the model performance, we collect special BCG signals including sinus arrhythmia data and post-exercise cardiac activities data, and analyze the reconstructed results. In conclusion, a BCG reconstruction algorithm is presented to solve the signal fading problem in the optical fiber interferometer innovatively, which greatly simplifies the BCG monitoring system.

1. Introduction

Long-term records and analysis of cardiac activity are essential in both clinic and home usage, especially for the aged and patients suffering from cardiovascular diseases. At present, electrocardiography (ECG) is one of the mainstream technologies used in cardiac monitoring. ECG reflects the electrical activity of the heart at a given moment, which is measured by attaching several electrodes to the skin. Each electrode pair is referred to as a lead and the 12-lead ECG is widely adopted in the clinic [1]. In recent years, the wearable ECG monitor has been developed for long-term monitoring [2]. Photoplethysmography (PPG) is another common cardiac monitoring way detected via the optic method [3]. A pulse oximeter attached to the finger can record the variational light intensity, which refers to the blood flow change derived from cardiac activities. However, ECG and PPG both belong to contact measurement, which may cause some problems in long-term monitoring such as skin allergy. Over the past decade, BCG proposed by Gordon [4] has regained the spotlight, owing to the fast-growing sensing techniques and signal processing methods. BCG is a vibration signal related to cardiac activity, which can be obtained in a non-invasive way. The vibration waveform represents body recoils produced by cardiac ejection during each heartbeat cycle. Similar to Q, R, S waves in ECG, BCG has I, J, K waves owning corresponding physiological significance. For example, the amplitude of the J wave is related to the aortic pulse pressure [5]. In addition, there are numerous studies on cardiovascular diseases detection that are based on BCG [6]. In view of the convenient measurement and medical application value, BCG is promising to be widely used for daily heartbeat monitoring.

#452408 https://doi.org/10.1364/OE.452408
Journal © 2022 Received 29 Dec 2021; revised 25 Mar 2022; accepted 25 Mar 2022; published 5 Apr 2022

Optics EXPRESS

In recent years, many sensing schemes have been proposed to detect BCG [7]. Among them, optical fiber sensors with the advantages of being immune to electromagnetic interference, lightweight and flexible have drawn much attention. For example, fiber Bragg grating strain sensors [8] and microbend optical fiber sensors [9] are adopted to fabricate the BCG monitors. However, the wavelength demodulator of the fiber Bragg grating sensor is expensive and complex, which is of no practical value in-home and clinic usage. For microbend optical fiber sensors, the sensitivity of it is limited and some details of BCG may lose. To overcome the mentioned weaknesses, our group concentrates on using the phase-sensitive optical fiber interferometer schemes to develop the vital signs monitors [10,11]. However, optical fiber interferometers have the problem of signal fading originated from environmental perturbations, which greatly degrades the performance of interferometers. It is the major problem encountered in our BCG monitoring system.

To solve the signal fading problem in optical fiber interferometers and obtain good-quality BCG recording with I, J, K waves, many modulation and demodulation technologies are adopted and investigated. For example, traditional schemes, such as 3×3 coupler-based demodulation and phase generated carrier technique, are introduced to reconstruct the heartbeat and breath signals [12–14]. Furthermore, we adopt the phase compensation method based on a close loop control system to address this problem in the previous work [15]. The mentioned schemes need additional hardware in the system. Therefore, we intend to reduce the complexity and cost of the hardware by replacing the modulator and demodulator with a reconstruction algorithm. In theory, the detected intensity signal is linear with BCG when the operating point is biased at the quadrature point (Q-point) in the interferometer. In practice, however, the operating point will deviate from Q-point due to the ambient noise, which results in the nonlinear problem in the detected signals. Because of the complex mathematical model caused by the dynamic drift of the operating point, it is difficult to develop a traditional algorithm to reconstruct BCG signals detected from an interferometer based on the intensity interrogation mode.

Deep learning algorithms have evolved rapidly recently and been widely employed in various fields [16]. Many deep learning models are successfully applied to BCG signal processing, such as heart/breath rate calculation and individual heartbeat detection [17,18]. In addition, reconstruction algorithms have also been extensively investigated based on the deep learning model. Among them, various models areapplied in the research of optical fiber devices to replace the traditional solutions. For example, deep neural networks, U-net, and GAN are adopted in the image reconstruction through the multi-mode fibers [19–21]. Convolutional neural networks are used for mode decomposition in the multi-mode fibers and few-mode fibers [22–24]. Inspired by these studies, we propose to adopt the GAN to build a reconstruction model. GANs are the common generative models, which can generate the desired distribution and improve the generative results through an adversarial process between generator and discriminator models [25]. pix2pix generative adversarial network (pix2pix GAN) is a variant of GAN [26]. Its generator has a structure of the encoder-decoder network, which can learn the mapping function and be used to build the reconstruction model. Although pix2pix GAN is a powerful model for two-dimension image processing, it cannot be directly applied to analyze the time-series signals, such as BCG.

Therefore, the present study is conducted to reconstruct signals from an optical fiber interferometer based on the intensity interrogation mode. A BCG reconstruction algorithm inspired by pix2pix GAN is proposed based on this purpose. To our knowledge, it is the first time to utilize an algorithm to solve the signal fading problem in the optical fiber interferometer-based BCG monitoring system. It means that additional phase modulators and demodulators are no longer needed in the interferometer. In our work, parameters of the neural network architecture are investigated and optimized, and several metrics are adopted to evaluate the accuracy of reconstructed BCG signals and I, J, K waves. Moreover, we test the performance of the BCG

Optics EXPRESS

reconstruction algorithm with two special BCG signals, which are of sinus arrhythmia data with specific heartbeat patterns and post-exercise data owning variational inter-beat intervals (IBIs), respectively. In conclusion, the proposed BCG reconstruction algorithm can solve the signal fading problem in optical fiber interferometers innovatively, which could be further applied in related applications, such as pulse waves reconstruction in the interferometer.

2. Method

2.1. Principle of BCG reconstruction in optical fiber interferometer

Our BCG monitoring system is an optical fiber MZI based on the intensity interrogation mode. As shown in Fig. 1(a), the optical system contains a distributed feedback (DFB) laser, an MZI-based BCG monitor, a photodetector (PD), and a data acquisition (DAQ) card. The optical fibers in the system are single-mode fibers (SMFs). BCG is a vibration signal that comes from body recoils resulting from cardiac activities. When subjects sit on the sensor, the phase change introduced by body recoils in the MZI can be detected by the optical intensity, which is referred to as raw BCG signals. Since the operating point deviates from the Q-point affected by the ambient noise, the obtained I, J, K waves in the BCG will be distorted. It makes the subsequent signal processing tasks difficult, such as heart rate (HR) calculation and heart rate variability (HRV) analysis. Instead of using complex modulation and demodulation devices to solve the problem, we propose to reconstruct BCG signals based on an algorithm by building a mapping model. The model can map raw signals to the BCG signal with standard I, J, K waves, which is called the reference BCG signal. As shown in Fig. 1(b), reference BCG signals can be collected by the reference system [15] and work as the ground truth. In addition to the MZI-based BCG monitor, the reference system has a phase compensation system to keep the operating point at Q-point.

The overview of the reconstruction method is shown in Fig. 1(c). We assume that the operating point of the raw BCG signal drifts to the red point in the change curve of optical intensity with phase. Meanwhile, the operating point of the reference system is kept at Q-point, which is the blue point in the curve. The output optical intensity of the MZI can be given as $I = A + B\cos(\varphi)$, where constants A and B are related to the light intensities of two arms in the MZI. We use x and y to represent the optical intensities of the raw BCG signal and the reference BCG signal, respectively. Therefore, x and y can be simplified to

$$x = \cos[\varphi_{BCG}(t) + \varphi_n(t)], \tag{1}$$

$$y = \cos[\varphi_{BCG}(t) + \varphi_n(t) + \varphi_{comp}(t)], \tag{2}$$

where $\varphi_{BCG}(t)$ and $\varphi_n(t)$ are phases introduced in the MZI by cardiac activities and ambient noise. $\varphi_{comp}(t) = 3\pi / 2 + 2n\pi - \varphi_n(t)$ is the phase introduced by the real-time phase compensation system, which keeps the operating point at the Q-point of rising edge by eliminating the $\varphi_n(t)$. Since the change curve of optical intensity with phase is approximately linear in the reference system, y can be obtained as $y \approx C\varphi_{BCG}(t)$, where C is a constant. The waveforms of x and y are shown in the green and blue lines in Fig. 1(c). We want to obtain y based on x but it is hard to be solved directly. Therefore, we propose to build the mapping model between x and y based on the deep learning method, which can be briefly described as

$$\hat{y} = f_\theta(x) \approx y, \tag{3}$$

where $f_\theta : \mathbb{R}^N \to \mathbb{R}^N$ is the mapping function and $\boldsymbol{\theta}$ contains the parameters in the mapping model, such as weights in the neural network. x and y are discretized by the DAQ card, and $\hat{y}$ is the reconstructed result based on x. The goal of the deep learning algorithm is to optimize $\boldsymbol{\theta}$ that minimizes the error between $\hat{y}$ and y.

Optics EXPRESS

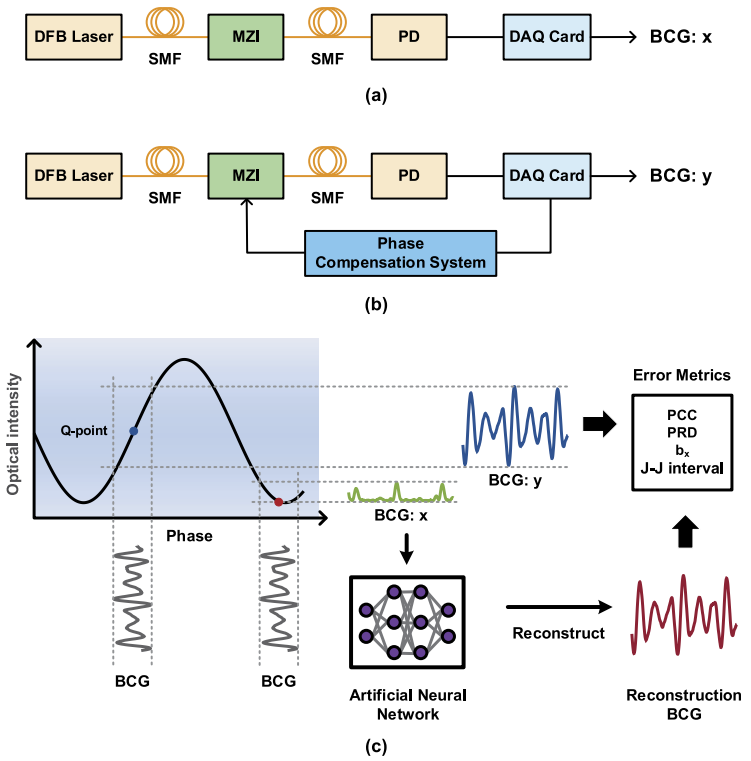

Fig. 1. The optical systems of (a) the BCG monitor and (b) the reference BCG monitor with a phase compensation system. (c) The overview of the reconstruction method.

2.2. *Deep learning-based BCG reconstruction algorithm*

The proposed deep learning-based BCG reconstruction algorithm is modified from pix2pix GAN. The pix2pix GAN is a kind of conditional generative adversarial network (conditional GAN) whose generator and discriminator are conditioned on the given information [27]. Compared to the typical conditional GAN which generates data based on some simple features, the generator structure in the pix2pix GAN is an encoder-decoder network and it can predict from pixels to pixels. Therefore, it can be used to build the mapping model between raw and reference BCG signals. However, pix2pix GAN is optimized in the image processing and it cannot be directly applied in the time domain signals. To cope with this, we modify the pix2pix GAN into a one-dimension (1D) model to fit the BCG reconstruction.

The modified model consists of a generator (G) and a discriminator (D). In our case, G learns the mapping between raw and reference BCG signals, and its input is raw BCG data and output is the reconstructed BCG result. D helps improve G's performance through the adversarial process. The training process of GAN is shown in Fig. 2(a) and there are three steps involved at each iteration. In step 1, D is trained to distinguish the true data with the input of reference data y. The label of y is 1, which means D is told that the input data are true. In step 2, D is trained to distinguish the fake data by feeding the generative data $G(x)$. $G(x)$ is generated by G based on raw data x. The label of $G(x)$ is 0 representing the fake input data. In step 3, we combinate D and G, and the parameters in D are frozen. $G(x)$ is fed into D with label 1, and thus G tries to generate data that is close to true data to fool D in this process. G will update its parameters in this step. In three steps, raw data x is paired with the input data fed into D to improve the

Optics EXPRESS

performance. The loss function in the network refers to [26], which can be shown as

$$L_{cGAN}(G,D) = \mathrm{E}_{x,y}[\log D(x,y)] + \mathrm{E}_x[\log(1 - D((x,G(x))))], \tag{4}$$

$$L_{L1}(G) = \mathrm{E}_{x,y}[||y - G(x)||_1], \tag{5}$$

$$G* = \arg\min_G \max_D L_{cGAN}(G,D) + \lambda L_{L1}(G), \tag{6}$$

where x, y and $G(x)$ are raw, reference and generated signals as mentioned. L_{cGAN} is the conditional GAN loss. L_{L1} is the Manhattan distance between reference and generated samples, which ensures that G is also trained to be close to the ground truth instead of only fooling D. Total loss $G*$ mixes the conditional GAN loss L_{cGAN} and the traditional Manhattan distance loss L_{L1} with weight λ.

The architecture of the BCG reconstruction algorithm is shown in Fig. 2(b). The network structure of G is similar to that of 1D U-net [28]. During the encoding step, the size of feature maps is compressed to half at each encoder block. The number of filter channels is double that of the previous encoder block, and the initial number is $\mathrm{n_f}$. The encoder block consists of a 1D strided convolutional layer with LeakyReLU [29] activation function followed by batch normalization. In the decoding stage, inversely, the size of the feature map doubles, and the channel halves at each symmetric decoder block. The skip connections are added between the symmetric layers in the encoding and decoding stages. Thus, the input size is equal to the output size, which is $\mathrm{N} \times 1$. $\mathrm{L_G}$ represents the number of encoder blocks in G, which is related to the performance of G. The network of D is a convolutional PatchGAN classifier, which penalizes the input at the scale of patches and averages all results as output. The $\mathrm{L_D}$ is the number of encoder blocks in D and the strided convolutional layer can adjust the size of the patch. In the experiment, we investigated various combinations of different values of $\mathrm{L_G}$ and $\mathrm{L_D}$ to optimize the model.

2.3. Experiment setup and data collection

To build the mapping model between raw and reference BCG signals, we packaged the mentioned two sensors together in a cushion, ensuring that raw and reference BCG signals can be detected simultaneously. In the data collection stage, the sensors are placed on a stable chair, and the subjects are asked to sit on it and keep still. The raw and reference signals from two sensors will be collected simultaneously by the DAQ card (National Instrument, USB6001) with a sampling rate of 1000 Hz, and then transferred to the computer for further processing, as shown in Fig. 3. We collected data from multiple healthy participants for a two-week period to make the mapping model more resistant to small variations like distinct sitting postures.

Since BCG signals cannot be detected when the subject is moving, the useless segments of signals caused by body movement are removed simultaneously in both raw and reference signals. The sampling rate of signals is reduced to 500 Hz in order to limit the peak of memory usage during training. A high-pass filter is applied to raw signals to eliminate the baseline drift. Since there is a slight time delay between the raw and reference signals due to the different working mechanisms of sensors, manual time calibration is needed. In addition, the raw and reference signals are divided into segments of consistent length $\mathrm{N} = 2048$ (4.096s duration) without overlapping and normalized to a range of -1 to 1. These data are used as a basic dataset to train and optimize the model.

2.4. Parameters selection and model evaluation

In the model, the reconstructed performance is affected by several parameters. Three metrics are adopted to estimate the model and optimize these parameters, including Pearson correlation coefficient (PCC), percent root mean square difference (PRD), and regression coefficient ($\mathrm{b_x}$) [30]. PCC refers to the correlative degree between reconstructed and reference BCG signals, and

Optics EXPRESS

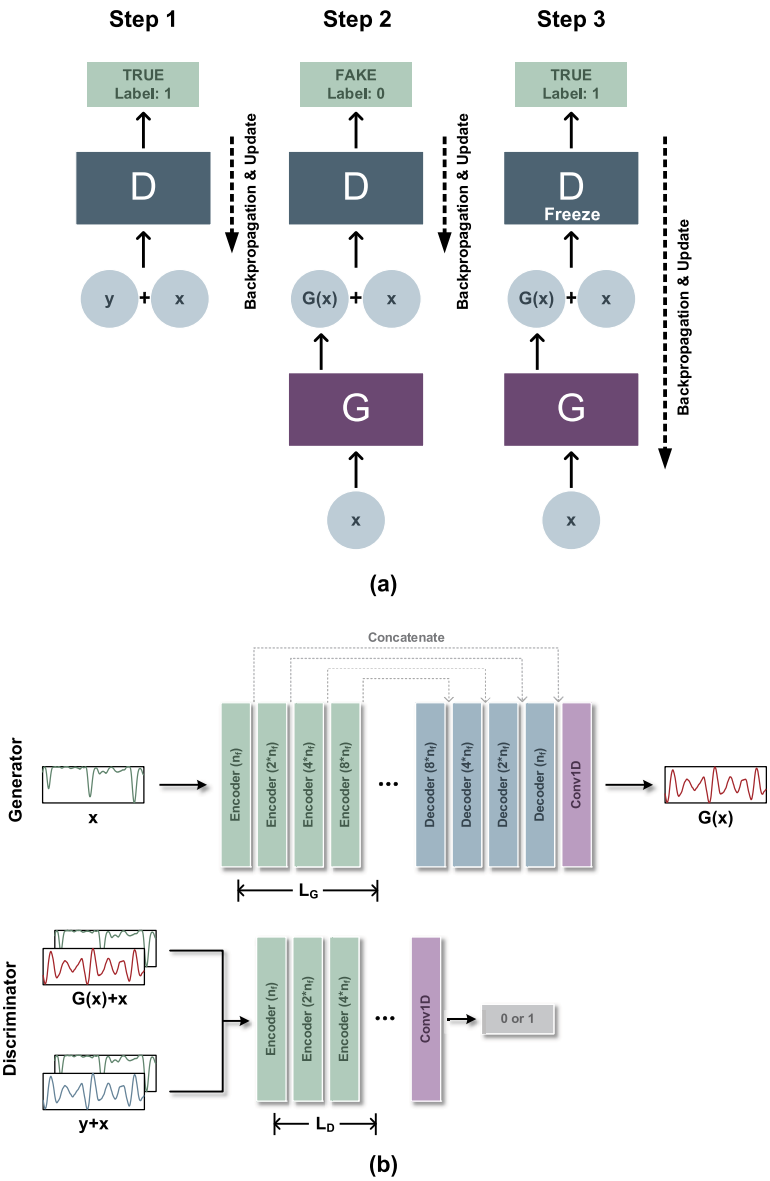

Fig. 2. (a) Training process of GAN. (b) Architecture of the BCG reconstruction algorithm.

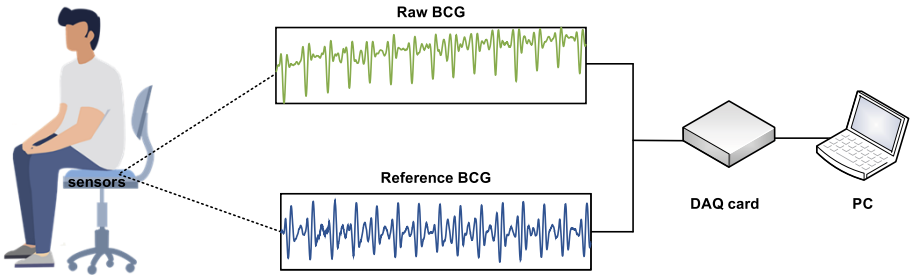

Fig. 3. The experiment setup.

Optics EXPRESS

a value of 1 indicates a strong positive correlation between the two signals. PRD represents the error between reconstructed and reference BCG signals and a smaller PRD means the higher performance of the reconstruction algorithm. Furthermore, b_x estimates the amplitude difference between the two BCG signals with a value closer to 1 being better. These metrics are shown in Eq. (7)-(9), where N is the number of samples, and G_x, y are reconstructed and reference BCG signals.

$$\mathrm{PCC} = \frac{\sum_{n=1}^{N}(G_x(n) - \overline{G_x})(y(n) - \bar{y})}{\sqrt{\sum_{n=1}^{N}(G_x(n) - \overline{G_x})^2}\sqrt{\sum_{n=1}^{N}(y(n) - \bar{y})^2}}, \tag{7}$$

$$\mathrm{PRD}\ (\%) = \sqrt{\frac{\sum_{n=1}^{N}(G_x(n) - y(n))^2}{\sum_{n=1}^{N}(y(n))^2}} \times 100, \tag{8}$$

$$b_x = \frac{\sum_{n=1}^{N} G_x(n)y(n)}{\sum_{n=1}^{N}(y(n))^2}. \tag{9}$$

Furthermore, another measure adopted to assess the model is based on the reconstructed IJK complex in BCG signals. IJK complex, consisting of I, J, and K waves, is the most visually obvious part of BCG. The I, J, and K waves can be used to estimate important cardiovascular parameters. As shown in Fig. 4, we use I, J, K waves and I', J', K' waves to distinguish the IJK complex in the reference and reconstructed BCG signals. The mean absolute error (MAE) between J-J intervals and J'-J' intervals is adopted as one metric to evaluate the time error of the IBI. Meanwhile, we use the error between I, J, K waves and I', J', K' waves as the additional metrics to evaluate the time delay of the reconstructed BCG signals.

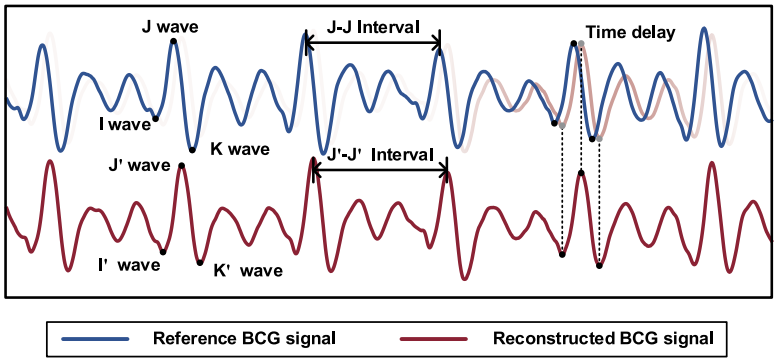

Fig. 4. I, J, K waves in the BCG signal.

2.5. *Special cases*

In the basic dataset, the heartbeat patterns are regular and HRs mainly range from 60 to 100 bpm. However, the BCG signals may become complex in some special cases. For example, the HR may exceed 100 bpm in the post-exercise condition. To evaluate the performance of the model in different scenarios, we collected special BCG signals including sinus arrhythmia data and post-exercise data, which own irregular heartbeat patterns and variational IBI, respectively. The details of reconstruction results are shown as follows.

Optics EXPRESS

3. Results and discussions

3.1. Basic dataset: training and analyzing

In the training process, since D usually converges faster than G, it is hard for the GAN model to balance G and D. If so, the model may fail to learn. Therefore, a series of parameters are investigated to balance the performance between G and D networks during the adversarial process and get a high-quality BCG reconstruction result. According to the preliminary experiment, some parameters are determined first. The kernel sizes of G and D networks are both 15×1, and the number of initial filter channel n_f in the first encoder block is 16. Adaptive moment estimation (Adam) [31] with a learning rate of 0.0002 is chosen as the optimizer in both G and D networks. Mini-batch gradient descent is adopted, and the batch size is 32. Weight λ in Eq. (6) is set as 100.

In the following experiment, the collected 7256 BCG segments are randomly divided into the training set and the test set, the ratio of which is 8 to 2. The test set has not been used in the preliminary experiment. Since the training loss cannot directly reflect the training phase of the GAN model, we display a batch of generative signals at a certain iteration cycle and calculate mentioned metrics based on the test set to evaluate the training progress. We set different combinations of block numbers in the G and D and monitor the model performance. Mean PCC, PRD, b_x, and MAE between reconstructed and reference signals in the test set with different values of L_G and L_D are shown in Table 1. We find that increasing the L_G value enhances the performance of the model greatly, while the L_D value affects less on the performance. The performance improves marginally when the L_G value is set to 8 and the size of the model grows dramatically. Therefore, we set the number of encoder and decoder block L_G as 7 in the G network, and L_D in the D network is set as 4.

Table 1. Mean PCC, PRD, b_x, and MAE in the test set with the combination of different numbers of blocks in G and D networks

L_G	L_D	PCC	PRD (%)	b_x	MAE
4	3	0.915	38.879	0.888	0.117
	4	0.920	38.004	0.897	0.115
5	3	0.926	36.459	0.899	0.113
	4	0.930	35.658	0.908	0.110
6	3	0.945	31.490	0.910	0.098
	4	0.943	32.007	0.912	0.100
7	3	0.952	29.683	0.918	0.093
	4	0.952	29.875	0.920	0.094
8	3	0.953	29.936	0.918	0.095
	4	0.953	29.838	0.922	0.094

As mentioned, two metrics are developed to verify the correctness of the reconstructed IJK complex in BCG signals. In the test set, the MAE between J-J intervals of reference BCG signals and J'-J' intervals of reconstructed BCG signals is 3.24 ms. The scatterplot of reconstructed J'-J' intervals versus reference J-J intervals is shown in Fig. 5(a). In addition, Fig. 5(b) is the box plot about absolute errors of time delay between I, J, K waves and I', J', K' waves, the median of which are all 2 ms. A small minority of the IJK complex, which are not detected in the reconstructed and reference segments, are excluded from the statistics. The results show the reconstructed IJK complex is closed to the reference IJK complex.

Then, the heartbeat patterns in the raw BCG signals with varying degrees of distortion are demonstrated. Figure. 6 is four common types of heartbeat patterns in the raw BCG signals. The inset picture is the change curve of optical intensity with phase in the MZI, and space α, β, χ, δ

Optics EXPRESS

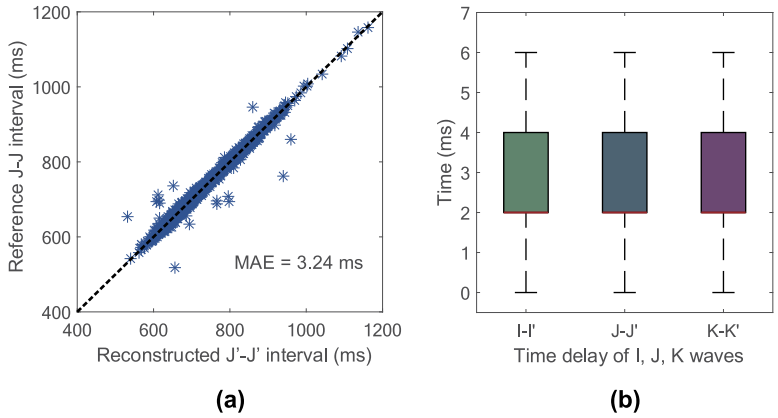

Fig. 5. (a) Scatterplot of reconstructed J'-J' intervals versus reference J-J intervals. (b) Box plot of absolute errors of time delay between I, J, K waves and I', J', K' waves.

are corresponding to positions where operating points are biased in Fig. 6(a) to (d), respectively. Among them, the green line in the first row represents raw BCG. Red and blue lines in the second row are the reconstructed BCG and reference BCG. In Fig. 6(a), the operating point is very close to the Q-point on the curve with a positive slope, and thus the raw signal is linearly positive with the reference BCG signal. As the operating point moves from space α to β, the raw signal has a nonlinearly positive correlation with the reference BCG signal, which results in signal distortion in Fig. 6(b). For Fig. 6(c), although the raw signal is linear with the reference BCG signal, it records reversal phase information, which is derived from the operating point being near the Q-point on the curve with a negative slope. Finally, the raw signal is nonlinearly negative with the reference BCG signal as the operating point drift to space δ, as shown in Fig. 6(d). It can be found that in either case, the reconstructed BCG is very close to the reference signal, and PCCs between the reconstructed and reference BCG signals in Fig. 6 are 0.974, 0.979, 0.980, and 0.976.

For the worst case, the pattern of the IJK complex in BCG signals is difficult to distinguish when the operating point drifts to the critical point (C-point in Fig. 6 inset picture), the waveforms of which are shown in Fig. 7. Based on the features of I, J, and K waves found in the raw signal, the mapping model can reconstruct the BCG signal. The PCCs of reconstructed BCG in Fig. 7 are 0.969 and 0.976, respectively. Furthermore, the BCG segments of subjects with different HRs are shown in Fig. 8(a) and (b). The model maintains high performance for both faster HR (97 bpm) and slower HR (66 bpm), in which the PCCs are 0.990 and 0.979, respectively.

The heartbeat patterns in the BCG change randomly with the drifting operating point. In addition, the number of heartbeat patterns in each segment depends on the HR of different subjects. Under such a complicated condition, the results show that the model has good adaptability to reconstruct BCG signals and the performance is satisfying, which means the BCG reconstruction algorithm can be used in further cardiac health analysis. Compared to the traditional modulation and demodulation methods, our method can reduce the hardware complexity in the system, which makes the sensor more portable. In further studies, we will try to reduce the complexity of the reconstruction algorithm. Moreover, to further validate the model, we also present the reconstructed BCG of two special cases collected in different scenarios in the following two parts.

3.2. Sinus arrhythmia

Sinus arrhythmia refers to an irregular heartbeat pattern that happened in healthy people, especially the young [32]. The cause of sinus arrhythmia is that the sinoatrial node does not pace the heart at a regular rate. Respiration is a common cause of sinus arrhythmia, which is called respiratory

Optics EXPRESS

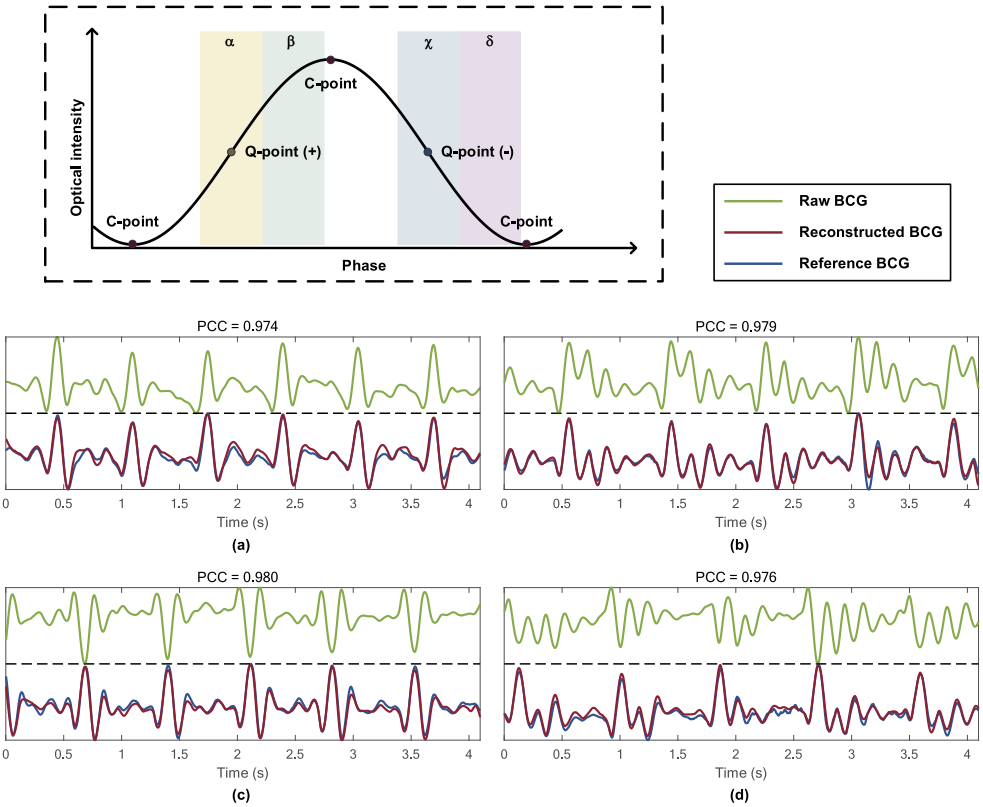

Fig. 6. Reconstructed BCG waveforms with different operating points in (a) to (d).

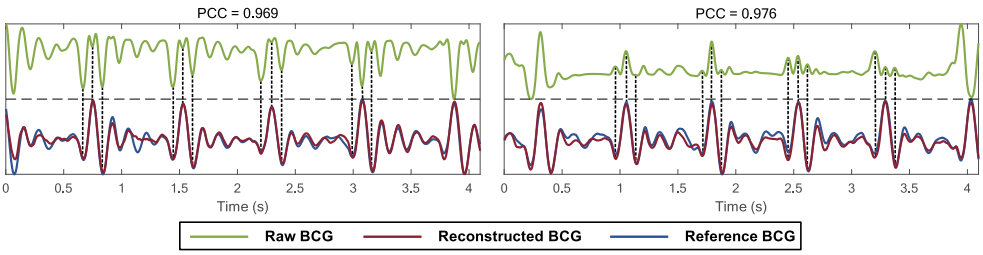

Fig. 7. Reconstructed BCG waveforms with poor quality of raw signals.

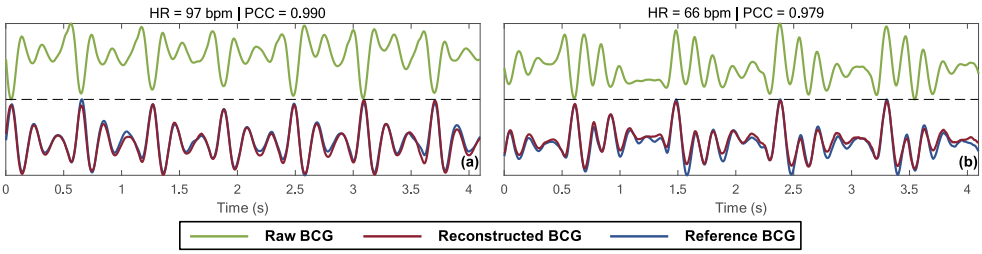

Fig. 8. Reconstructed BCG waveforms with different HRs: (a) HR is 97 bpm and (b) HR is 66 bpm.

Optics EXPRESS

sinus arrhythmia. The HR usually fluctuates in the process of breathing derived from the change in vagal tone during different respiratory phases. Therefore, respiratory sinus arrhythmia is a significant indicator related to cardiac vagal function.

In the experiment, we found that a few irregular heartbeat patterns are collected from one subject. Therefore, we made the subject wear an ECG monitor (SparkFun, AD8232) and sit on the sensor to collect ECG, raw BCG, and reference BCG simultaneously. Finally, we detected some heartbeat segments with sinus arrhythmia and fed them into the model. Part of the results is shown in Fig. 9, in which the red, blue and purple lines represent the reconstructed BCG, reference BCG, and ECG separately. The grey dotted boxes show the irregular heartbeat patterns in collected signals. According to the ECG patterns, the presented segments are identified as sinus arrhythmia. The PCC between the reconstructed and reference segments are 0.915 and 0.932 in Fig. 9. Although the PCC decreases a bit compared to that of the normal BCG reconstructed segment, the reconstruction algorithm still works well.

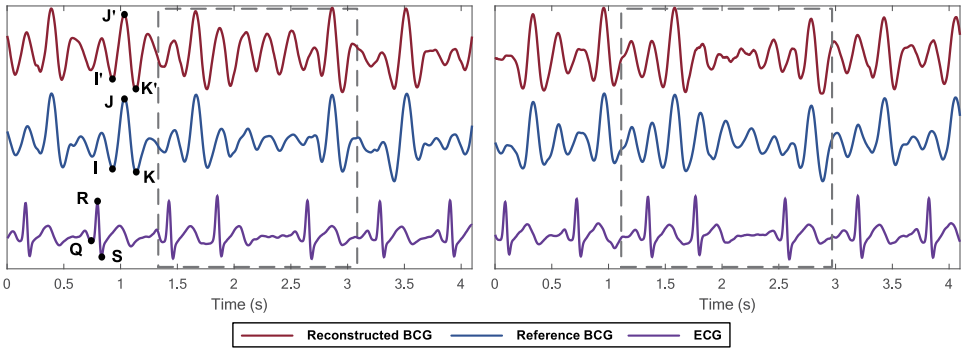

Fig. 9. Reconstructed BCG, reference BCG, and ECG segments with sinus arrhythmia.

3.3. Post-exercise physiological activities characterization

HRV refers to the temporal variation between the time intervals of consecutive heartbeats, which originates from the autonomic nervous system of humans [33]. These temporal variations are in connection with a variety of physiological disorders, and thus HRV is a significant indicator to access the physical condition, especially cardiac health. IBI, which is the time interval between individual heartbeats, is used to measure the HRV. Officially, the R-R interval time series in ECG is recommended as the reference IBI. Furthermore, the J-J interval time series in BCG has also been successfully validated as IBI for HRV analysis during post-exercise conditions [34].

Exercise is a noninvasive method to alter the time interval of heartbeats and is widely used in HRV analysis experiments [35]. In our work, we conducted the experiment of post-exercise BCG signals collection to test the performance of the model in variational IBI reconstruction. During data collection, one subject whose BCG data were not included in the basic dataset, was asked to run for 3 minutes. After that, the post-exercise BCG and ECG signals were collected simultaneously for 5 minutes by the sensors. Totally, we collected 554 heartbeats, and among them, 551 heartbeats were successfully reconstructed. Three segments of reconstructed post-exercise BCG segments are shown in Fig. 10(a). It can be found that the HR drops gradually from 153 bpm to 107 bpm after 3 minutes. Figure. 10(b) shows the post-exercise IBI variation of BCG and ECG in 5 minutes, of which the R-R time interval in the ECG is used as the reference IBI. The PCC between the BCG IBI variation and ECG IBI variation is 0.985, which shows the reconstructed IBI variations are close to the reference values.

Optics EXPRESS

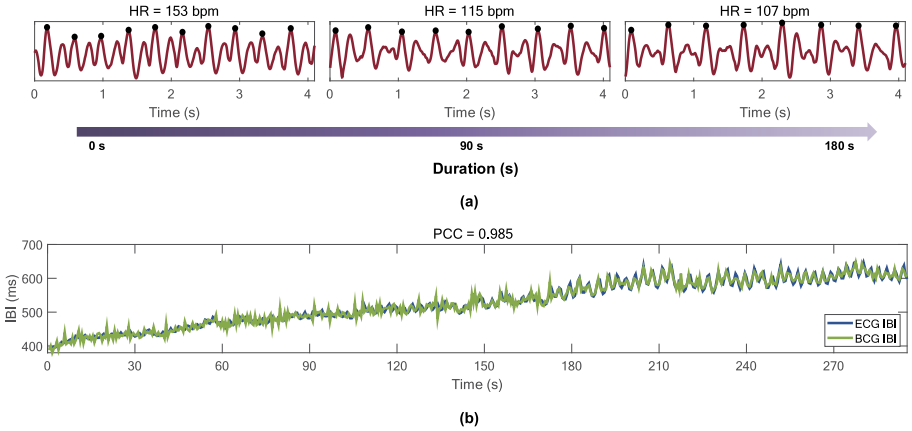

Fig. 10. (a) The reconstructed post-exercise BCG segments during 3 minutes. (b) The post-exercise IBI variation of BCG and ECG during 5 minutes.

4. Conclusion

In this paper, we have presented a BCG reconstruction algorithm based on the modified pix2pix GAN, which can retrieve BCG signals by solving signal fading problems in the MZI without using any additional hardware. This model greatly reduces the cost and complexity of the BCG monitoring system. The reconstructed BCG signals in the test data achieve satisfying results, of which the mean PCC, PRD, b_x, and MAE are 0.952, 29.875, 0.920, and 0.094, respectively. In addition, we collected special BCG data including sinus arrhythmia data and post-exercise data, and the model can reconstruct these BCG data in high performance. The BCG reconstruction algorithm creatively solves the signal fading problem in the interferometer, and it could be further applied in related applications, such as pulse waves reconstructed from the interferometer.

Funding. National Natural Science Foundation of China (61971372); University Grants Committee (Grant 15200718).

Disclosures. The authors declare no conflicts of interest.

Data availability. Data underlying the results presented in this paper are not publicly available at this time but may be obtained from the authors upon reasonable request.

References

1. P. Kligfield, L. S. Gettes, J. J. Bailey, R. Childers, B. J. Deal, E. W. Hancock, G. V. Herpen, J. A. Kors, P. Macfarlane, D. M. Mirvis, O. Pahlm, P. Rautaharju, and G. S. Wagner, "Recommendations for the standardization and interpretation of the electrocardiogram: part I: the electrocardiogram and its technology a scientific statement from the American Heart Association Electrocardiography and Arrhythmias Committee, Council on Clinical Cardiology; the American College of Cardiology Foundation; and the Heart Rhythm Society endorsed by the International Society for Computerized Electrocardiology," J. Am. Coll. Cardiol. **49**(10), 1109–1127 (2007).
2. E. Nemati, M. J. Deen, and T. Mondal, "A wireless wearable ECG sensor for long-term applications," IEEE Commun. Mag. **50**(1), 36–43 (2012).
3. S. A. Mascaro and H. H. Asada, "Photoplethysmograph fingernail sensors for measuring finger forces without haptic obstruction," IEEE Trans. Robot. Automat. **17**(5), 698–708 (2001).
4. J. W. Gordon, "Certain molar movements of the human body produced by the circulation of the blood," J. Appl. Physiol. **11**(Pt 3), 533–536 (1877).
5. C. S. Kim, S. L. Ober, M. S. Mcmurtry, B. A. Finegan, O. T. Inan, R. Mukkamala, and J. O. Hahn, "Ballistocardiogram: Mechanism and Potential for Unobtrusive Cardiovascular Health Monitoring," Sci. Rep. **6**(1), 31297 (2016).
6. X. Wen, Y. Huang, X. Wu, and B. Zhang, "A feasible feature extraction method for atrial fibrillation detection from BCG," IEEE J. Biomed. Health Inform. **24**(4), 1093–1103 (2020).
7. O. T. Inan, P. F. Migeotte, K. S. Park, M. Etemadi, K. Tavakolian, R. Casanella, J. Zanetti, J. Tank, I. Funtova, G. K. Prisk, and M. Di Rienzo, "Ballistocardiography and seismocardiography: A review of recent advances," IEEE J. Biomed. Health Inform. **19**(4), 1414–1427 (2015).
8. Ł. Dziuda, M. Krej, and F. W. Skibniewski, "Fiber Bragg grating strain sensor incorporated to monitor patient vital signs during MRI," IEEE Sens. J. **13**(12), 4986–4991 (2013).

Optics EXPRESS

9. Z. Chen, J. Hu, and C. Yu, "Fiber senor for long-range and biomedical measurements," in 2013 *12th International Conference on Optical Communications and Networks (ICOCN)*, 1–4 (2013).
10. C. Yu, W. Xu, N. Zhang, and C. Yu, "Non-invasive smart health monitoring system based on optical fiber interferometers," in 2017 *16th International Conference on Optical Communications and Networks (ICOCN)*, 1–3 (2017).
11. F. Tan, W. Lyu, S. Chen, Z. Liu, and C. Yu, "Contactless vital signs monitoring based on few-mode and multi-core fibers," Opto-Electron. Adv. **3**(5), 190034 (2020).
12. S. Wang, X. Ni, L. Li, J. Wang, Q. Liu, Z. Yan, L. Zhang, and Q. Sun, "Noninvasive monitoring of vital signs based on highly sensitive fiber optic mattress," IEEE Sens. J. **20**(11), 6182–6190 (2020).
13. W. Lyu, W. Xu, F. Yang, S. Chen, F. Tan, and C. Yu, "Non-invasive Measurement for Cardiac Variations Using a Fiber Optic Sensor," IEEE Photonics Technol. Lett. **33**(18), 990–993 (2021).
14. F. Yang, W. Lyu, C. Pan, S. Yang, F. Tan, S. Chen, and C. Yu, "Contactless vital signs monitoring based on optical fiber Mach-Zehnder interferometer aided with passive homodyne demodulation methods," in 2020 *Asia Communications and Photonics Conference (ACP)*, M4A-79 (2020).
15. S. Chen, F. Tan, W. Lyu, and C. Yu, "Ballistocardiography monitoring system based on optical fiber interferometer aided with heartbeat segmentation algorithm," Biomed. Opt. Express **11**(10), 5458–5469 (2020).
16. W. Rawat and Z. Wang, "Deep convolutional neural networks for image classification: A comprehensive review," Neural Computation **29**(9), 2352–2449 (2017).
17. Q. Wang, Y. Zhang, G. Chen, Z. Chen, and H. I. Hee, "Assessment of heart rate and respiratory rate for perioperative infants based on ELC model," IEEE Sens. J. **21**(12), 13685–13694 (2021).
18. S. Tahir, I. Sadek, and B. Abdulrazak, "A CNN-ELM-Based Method for Ballistocardiogram Classification in a Clinical Environment," in 2021 *IEEE Canadian Conference on Electrical and Computer Engineering (CCECE)*, 1–6 (2021).
19. C. Zhu, E. A. Chan, Y. Wang, W. Peng, R. Guo, B. Zhang, C. Soci, and Y. Chong, "Image reconstruction through a multimode fiber with a simple neural network architecture," Sci. Rep. **11**(1), 1–10 (2021).
20. N. Borhani, E. Kakkava, C. Moser, and D. Psaltis, "Learning to see through multimode fibers," Optica **5**(8), 960–966 (2018).
21. Z. Yu, Z. Ju, X. Zhang, Z. Meng, F. Yin, and K. Xu, "High-speed multimode fiber imaging system based on conditional generative adversarial network," Chin. Opt. Lett. **19**(8), 081101 (2021).
22. Y. An, L. Huang, J. Li, J. Leng, L. Yang, and P. Zhou, "Learning to decompose the modes in few-mode fibers with deep convolutional neural network," Opt. Express **27**(7), 10127–10137 (2019).
23. S. Rothe, Q. Zhang, N. Koukourakis, and J. Czarske, "Intensity-only mode decomposition on multimode fibers using a densely connected convolutional network," J. Lightwave Technol. **39**(6), 1672–1679 (2021).
24. S. Rothe, Q. Zhang, N. Koukourakis, and J. W. Czarske, "Deep learning for computational mode decomposition in optical fibers," Appl. Sci., **10**(4), 1367 (2020).
25. I. J. Goodfellow, J. Pouget-Abadie, M. Mirza, B. Xu, D. Warde-Farley, S. Ozairy, A. Courville, and Y. Bengio, "Generative Adversarial Nets," arXiv, 1406.2661 (2014).
26. P. Isola, J.-Y. Zhu, T. Zhou, and A. A. Efros, "Image-to-Image Translation with Conditional Adversarial Networks," in 2017 *Proceedings of the IEEE conference on computer vision and pattern recognition*, 1125–1134 (2017).
27. M. Mirza and S. Osindero, "Conditional Generative Adversarial Nets," arXiv, 1411.1784 (2014).
28. O. Ronneberger, P. Fischer, and T. Brox, "U-Net: Convolutional Networks for Biomedical Image Segmentation," in 2015 *International Conference on Medical image computing and computer-assisted intervention*, 234–241 (2015).
29. B. Xu, N. Wang, T. Chen, and M. Li, "Empirical evaluation of rectified activations in convolutional network," arXiv, 1505.00853 (2015).
30. J. Lee, K. Oh, B. Kim, and S. K. Yoo, "Synthesis of electrocardiogram V-lead signals from limb-lead measurement using R-peak aligned generative adversarial network," IEEE J. Biomed. Health Inform. **24**(5), 1265–1275 (2020).
31. D. P. Kingma and J. Ba, "Adam: A method for stochastic optimization," arXiv, 1412.6980 (2014).
32. G. G. Berntson, J. T. Cacioppo, and K. S. Quigley, "Respiratory sinus arrhythmia: autonomic origins, physiological mechanisms, and psychophysiological implications," Psychophysiology **30**(2), 183–196 (1993).
33. J. Sztajzel, "Heart rate variability: a noninvasive electrocardiographic method to measure the autonomic nervous system," Swiss Med. Wkly. **134**(35-36), 514–522 (2004).
34. A. J. Camm, M. Malik, J. T. Bigger, G. Breithardt, S. Cerutti, R. J. Cohen, P. Coumel, E. L. Fallen, H. L. Kennedy, R. E. Kleiger, L. Federico, M. Alberto, A. J. Moss, J. N. Rottman, G. Schmidt, P. J. Schwartz, and D. H. Singer, "Heart rate variability. Standards of measurement, physiological interpretation, and clinical use. Task Force of the European Society of Cardiology and the North American Society of Pacing and electrophysiology," Eur. Heart J. **17**(3), 354–381 (1996).
35. M. Javorka, I. Zila, T. Balhárek, and K. Javorka, "Heart rate recovery after exercise: relations to heart rate variability and complexity," Braz. J. Med. Biol. Res. **35**(8), 991–1000 (2002).